Park *et al.*
Journal of Analytical Science and Technology (2022) 13:51
https://doi.org/10.1186/s40543-022-00359-w

Journal of Analytical Science and Technology

RESEARCH ARTICLE

Open Access

Investigation of Cd(II) sorption by mackinawite (FeS) under anoxic conditions

Minji Park[1], Kwang-Sik Lee[2], Jungho Ryu[3], Young-Suk Song[3] and Hoon Young Jeong[1*]

Abstract

Mackinawite (FeS) was investigated for cadmium ion (Cd(II)) sorption under anoxic conditions. At the surface loading of Cd(II) (i.e., $[Cd(II)]_0/[FeS]_0$) ≤ 5 mmol/g, FeS quantitatively immobilized Cd(II). Adsorption and CdS precipitation were responsible for Cd(II) uptake, with their relative importance depending on $[Cd(II)]_0/[FeS]_0$. At pH 5.5–6.0, adsorption was more important when $[Cd(II)]_0/[FeS]_0$ ≤ 0.05 mmol/g. According to energy dispersive X-ray spectroscopy, Cd(II) exhibited strong spatial correlations with S and Cl. While Cd-S correlations corresponded to CdS precipitation and/or the surface complexation of Cd(II) with sulfhydryl functional sites, Cd–Cl correlations indicated the presence of chloride-complexed Cd(II). Given the strong correlations of both pairs, the adsorbed Cd(II) was likely present in chlorosulfide forms (e.g., ≡FeS–Cd(II)–Cl). When $[Cd(II)]_0/[FeS]_0$ exceeded 0.05 mmol/g, CdS precipitation became more important. X-ray diffraction, transmission electron microscopy, and selected area electron diffraction revealed the formation of hawleyite (cubic CdS) at higher surface loadings. The Fe(II) species liberated during CdS precipitation were resorbed through adsorption at acidic pH and the formation of Fe (oxyhydr)oxides at neutral to basic pH. Given the greater stability of CdS than adsorbed Cd(II), the prevalence of the former suggests that FeS can serve as an effective reagent to remedy Cd(II) contamination under anoxic conditions. Due to its ubiquitous presence, FeS may also control the environmental fate and mobility of Cd(II) in sulfidic sediments.

Keywords: Mackinawite, Cadmium, Hawleyite, Sorption

Introduction

Cadmium is an environmental concern because of its high toxicity and mobility (Genchi et al. 2020; Kubier et al. 2019; Moore and Ramamoorthy 1984). Its adverse health effects include anemia, osteoporosis, renal damage, and Itai–Itai disease (Kubier et al. 2019; Lusvardi et al. 2002). Although many heavy metal ions form stable hydroxide phases at circumneutral pH, $Cd(OH)_2$ is highly soluble under such conditions, posing a great challenge for its sequestration in aquatic environments (Bostick et al. 2000; Kubier et al. 2019). Elevated Cd contamination is mainly derived from anthropogenic sources including mining, metallurgy, battery production, and chemical stabilizers (Larison et al. 2000).

Most studies related to Cd(II) removal have focused on its sorption to (oxyhydr)oxides and clay minerals under oxic conditions (Chen et al. 1997; Malferrari et al. 2007; Panuccio et al. 2009; Papelis 1995; Tan et al. 2016). The weak association with these phases may cause previously sorbed Cd(II) to be prone to remobilization (Bostick et al. 2000; Kubier et al. 2019; Tan et al. 2016). Under anoxic conditions, sulfate-reducing bacteria produce dissolved sulfides, which react with (hydr)oxide minerals to form sulfide minerals (Goldhaber and Kaplan 1974). Due to the natural abundance of Fe, the dominant products in sulfidic sediments are usually Fe sulfides such as mackinawite (FeS), greigite (Fe_3S_4), and pyrite (FeS_2) (Morse and Arakaki 1993). Among them, mackinawite is the major constituent of acid-volatile sulfides (AVS) (Rickard 1974). This mineral, which eventually transforms

*Correspondence: hjeong@pusan.ac.kr

[1] Department of Geological Sciences, BK21 School of Earth and Environmental Systems, Pusan National University, Busan 46241, South Korea
Full list of author information is available at the end of the article

into more stable phases (e.g., greigite and pyrite), can persist in sulfidic sediments for a long period (Benning et al. 2000). Due to its chalcophilic nature, Cd(II) tends to be sequestered through precipitation as sulfide minerals by reaction with FeS (Coles et al. 2000; Jeong and Hayes 2003). Notably, AVS is important in determining the toxicity and bioavailability of Cd in anoxic sediments (Di Toro et al. 1990, 1996). Considering its ubiquitous presence and long-term stability in anoxic sediments, mackinawite is critical for predicting the fate of Cd(II) in subsurface environments. Recently, thiol-functionalized silica, graphene oxide, magnetite, and biochar have been used to treat Cd(II)-contaminated water (Chen et al. 2020; Liang et al. 2009; Pirveysian and Ghiaci 2018; Song et al. 2022). Due to the strong interaction of S(-II) with Cd(II), these functionalized materials provided greater sorption capacities for Cd(II) compared to pristine materials (Chen et al. 2020; Pirveysian and Ghiaci 2018; Song et al. 2022).

Although Fe sulfides have been shown to effectively immobilize Cd(II) under anoxic conditions (Bostick et al. 2000; Coles et al. 2000; Jean and Bancroft 1986; Parkman et al. 1999), the sorption mechanisms under various geochemical conditions remain unclear. The possible mechanisms include adsorption (surface complexation at a low surface loading and surface precipitation at a high surface loading), CdS precipitation, and the formation of solid solutions ([Cd,Fe]S) (Coles et al. 2000; Jeong et al. 2007). By reaction with pyrite, Bostick et al. (2000) found that Cd(II) was sequestered by forming CdS. Coles et al. (2000) investigated the uptake of Cd(II) by mackinawite (FeS). They proposed the formation of [Cd,Fe]S through the lattice exchange of Cd(II) for Fe(II) on the FeS surface at a Cd(II) surface loading ($[Cd(II)]_0/[FeS]_0$) < 4 mmol/g. They also postulated that Cd(II) could be immobilized through adsorption onto the aforementioned mixed sulfide at a higher surface loading. However, Framson and Leckie (1978) reported that Cd(II) does not co-precipitate with FeS. By reaction with FeS, Jeong et al. (2007) found that Hg(II) was sequestered by both adsorption and HgS precipitation. In their study, the former mechanism was dominant at a low Hg(II) surface loading ($[Hg(II)]_0/[FeS]_0$) < 0.5 mmol/g. Similar sorption behaviors are expected for Cd(II) sorption by FeS because Cd(II) and Hg(II) form more insoluble metal sulfides than FeS (Stumm and Morgan 1995). Due to the significantly higher surface loadings of Cd(II) ($[Cd(II)]_0/[FeS]_0$) ≥ 2.22 mmol/g), Coles et al. (2000) did not recognize the occurrence of adsorption. Even at $[Cd(II)]_0/[FeS]_0$ = 0.5 mmol/g, Parkman et al. (1999) did not identify adsorbed Cd(II) species by Cd K-edge X-ray absorption spectroscopy (XAS) analysis. However, Özverdi and Erdem (2006) reported that adsorption was mainly responsible for Cd(II) removal by FeS at the pH values of 3–6. Thus, the sorption behaviors of Cd(II) by FeS are seemingly complex and condition-specific.

This study aims to elucidate the Cd(II) sorption mechanisms by nanocrystalline mackinawite (FeS) under anoxic conditions. A series of batch experiments were performed as a function of $[Cd(II)]_0/[FeS]_0$ and pH. The resultant sorption products were subjected to X-ray diffraction (XRD) and transmission electron microscopy (TEM) coupled with energy dispersive X-ray spectroscopy (EDS). Additionally, to obtain a comprehensive understanding of Cd(II) sorption, our results were compared to those of Hg(II) sorption from Jeong et al. (2007, 2020).

Material and methods

Unless otherwise specified, anoxic conditions were maintained for all experiments. Mackinawite synthesis and sorption experiments were conducted inside an anaerobic chamber (Coy Inc., Grass Lake, MI) with an atmospheric composition of ~ 5% H_2 in N_2. After Milli-Q water was deoxygenated by boiling and purging with N_2, it was equilibrated inside the anaerobic chamber for at least one day before use. Solutions for mackinawite synthesis and sorption experiments were prepared using deoxygenated water.

FeS synthesis

FeS was prepared by combining Fe(II) and S(-II) solutions (Jeong et al. 2008). In brief, 2.0 L of a $FeCl_2$ solution (0.57 M) was mixed with 1.2 L of a N_2S solution (1.1 M) to form black precipitates. The resultant suspensions were aged on a magnetic stirrer for three days. After centrifugation at 10,000 rpm for 20 min, the supernatant was decanted and the remaining paste was rinsed with deoxygenated water. For this, the bottles were sealed with silicon gaskets to minimize oxygen exposure. The rinsing procedure was repeated eight times to remove the residual salts. Finally, the paste was freeze-dried under a vacuum. Previously, freeze-drying was avoided to keep FeS particles hydrated and dispersed (Wilkin and Beak 2017). However, changes in the surface properties of mackinawite due to freeze-drying were recovered by particle resuspension (Ohfuji and Rickard 2006). Moreover, suspended FeS particles were enlarged through an aggregation-growth mechanism (Guilbaud et al. 2010). Thus, freeze-drying was necessary to maintain the surface properties. The freeze-dried particles were ground in a mortar and sealed in glass vials capped with Teflon-coated rubber septa until use. As characterized by broad reflection peaks (Additional file 1: Fig. S1), the synthesized FeS was nanocrystalline mackinawite with a specific surface area of 284 m^2/g (Jeong et al. 2008).

Sorption experiments

Sorption experiments were conducted using 12 mL polypropylene tubes. Different amounts of FeS were weighed into tubes to obtain the initial FeS concentrations ($[FeS]_0$) of 2, 5, and 10 g/L. Then, $CdCl_2$ stock solutions were added to the tubes to obtain the initial Cd(II) concentrations ($[Cd(II)]_0$) of 0.0005–0.02 M. Consequently, the surface loading of Cd(II) ($[Cd(II)]_0/[FeS]_0$) ranged from 0.05 to 10 mmol/g. The sorption mechanisms are controlled by the surface loadings, not the initial metal concentrations (Coles et al. 2000; Jeong et al. 2007; Wilkin and Beak 2017). Thus, our data interpretation was based on $[Cd(II)]_0/[FeS]_0$. Subsequently, HCl or NaOH solutions were added to have the final pH of 4.0–11.0. Then, NaCl solutions were added to obtain a total chloride concentration (Cl_T) of 0.2 M. A high Cl concentration was required to minimize the difference in ionic strength among batches and facilitate the separation of the solution phase from the suspended particles (Jeong et al. 2007). Consequently, the results of this study are relevant to brackish and saline environments (e.g., brackish aquifers, estuaries, and marine sediments). Finally, deoxygenated water was added to the tubes to obtain a volume of 10 mL. Triplicates were prepared for the selected batches to estimate experimental errors. Also, controls without FeS were run to account for possible losses from the sorption of Cd(II) to the tubes. The resultant batches were agitated on a reciprocal shaker at room temperature for 48 h, which was sufficient to reach the equilibrium state for both adsorption and metal sulfide precipitation (Additional file 1: Fig. S2).

Following the reaction period, a portion of the supernatants were filtered using 0.2 or 0.05 μm polypropylene filter (Whatman). While the former filter retained all aggregates of suspended particles in the batches at pH < ~10.0 (Jeong et al. 2007), the latter was required for the batches at pH > ~10.0 due to the formation of highly dispersed CdS precipitates. After a portion of the filtrates were acidified with 10% HNO_3, dissolved Cd and Fe concentrations were measured on an inductively coupled plasma with an optical emission spectrometry (ICP-OES, Perkin-Elmer) and a mass spectrometry (ICP-MS, Perkin-Elmer), respectively. Quality controls for ICP-OES and ICP-MS analyses were conducted by applying multiple runs, serial dilutions, and calibration standards. Additionally, several emission lines of Fe were collected by ICP-OES to check spectral interference, and ^{59}Co was used as an internal standard for ICP-MS analysis of ^{114}Cd. The detection limit of dissolved Cd was ~2 ppb (3.56×10^{-8} M), which was lower than the maximum contamination level set by the U.S. EPA (5 ppb). The remaining, unacidified filtrates were measured for the final (equilibrium) pH. After centrifugation, the wet pastes were collected for TEM analysis. Also, fractions of the wet slurries were subsequently freeze-dried for XRD analysis.

XRD and TEM

XRD patterns were collected on a Rigaku 12 kW rotating anode generator with Cu-K_α radiation at 40 kV and 100 mA. To assess the sample alteration (e.g., oxidation) during XRD measurements, reflection patterns were obtained for both the freeze-dried samples and those that had been wetted with glycerin after being freeze-dried. The XRD data were obtained from 10° to 70° 2θ with an angular increment of 0.02° at a scanning rate of 2° 2θ per min.

To obtain a sufficient emission intensity of Cd for elemental mapping, TEM analyses were limited to the batches at a high surface loading ($[Cd(II)]_0/[FeS]_0 = 7.5$ mmol/g). For this, portions of the wet pastes were resuspended in a 90% ethanol solution inside the anaerobic chamber. Aliquots of the suspensions were applied to a holey carbon film supported by a copper mesh grid. The TEM grids were then stored inside N_2-filled bags and transferred to a high-vacuum TEM chamber. TEM analyses were conducted using a JEOL 2010F analytical electron microscope at 200 kV with an energy dispersive X-ray spectrometer. TEM analyses included the high-angle annular dark-field scanning TEM (HAADF-STEM), high-resolution TEM (HR-TEM), selected area electron diffraction (SAED), and EDS with a spatial resolution of ~1.7 Å.

Results and discussion

Cd(II) sorption

Nearly all of the initially added Cd(II) ($[Cd(II)]_0 = 0.0005$–0.02 M) was immobilized in the batches containing 5 or 10 g/L of FeS (Additional file 1: Fig. S3), with the dissolved Cd(II) concentrations ($[Cd(II)]_{diss}$) below the detection limit (~2 ppb). However, in 2 g/L FeS batches, $[Cd(II)]_{diss}$ was above the detection limit at $[Cd(II)]_0 = 0.015$ and 0.02 M (Fig. 1a). Thus, FeS can quantitatively immobilize Cd(II) at $[Cd(II)]_0/[FeS]_0 \leq 5$ mmol/g. Similarly, FeS was effective in immobilizing Ni(II), Cd(II), Pb(II), Sn(II), and Hg(II) (Coles et al. 2000; Dulnee and Scheinost 2015; Jeong et al. 2007; Wilkin and Beak 2017).

In Fig. 1b, the dissolved Fe(II) concentration ($[Fe(II)]_{diss}$) is shown as a function of $[Cd(II)]_0$ in 10 g/L FeS batches. Notably, $[Fe(II)]_{diss}$ increases in proportion to $[Cd(II)]_0$ at pH < ~7. A similar pattern was observed for the sorption of Hg(II) and Ni(II) by FeS (Jeong et al. 2007; Wilkin and Beak 2017). Considering the nearly quantitative removal of Cd(II), the following reactions can lead to the liberation of Fe(II) from FeS with the formation of metal sulfides:

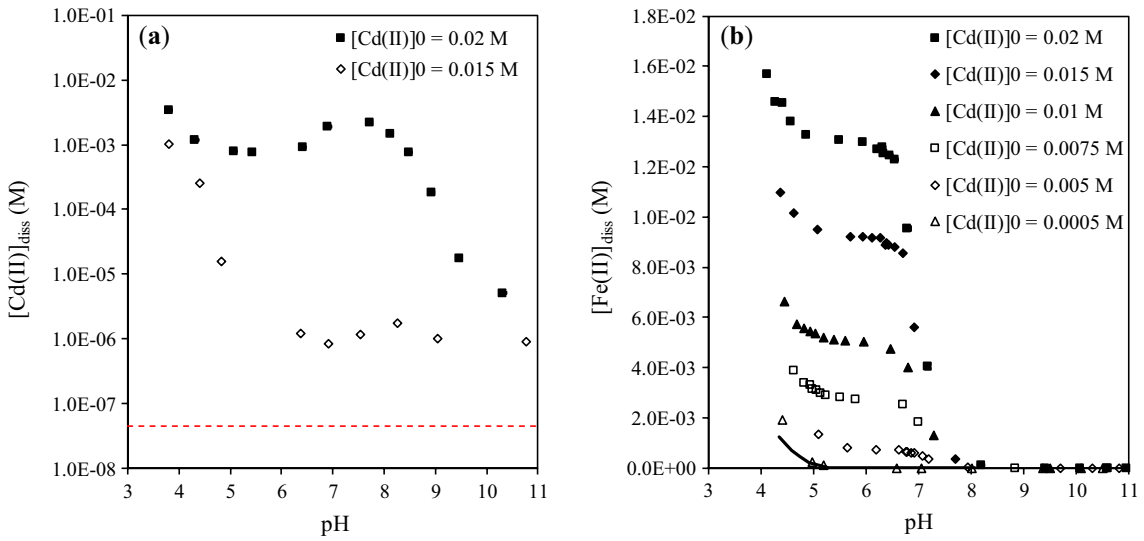

Fig. 1 Dissolved Cd(II) concentration ($[Cd(II)]_{diss}$) as a function of initial Cd(II) concentration ($[Cd(II)]_0$) in 2 g/L FeS batches (**a**) and dissolved Fe(II) concentration ($[Fe(II)]_{diss}$) as a function of $[Cd(II)]_0$ in 10 g/L FeS batches (**b**). In part **a**, the dashed line represents the maximum contamination level (MCL, 5 ppb) according to U.S. EPA. In part **b**, the solid line represents the solubility of FeS, which was directly measured from FeS batches in the absence of Cd(II)

- Formation of M^{2+}-substituted FeS by lattice exchange on the FeS surface

$$FeS(s) + xM(II) \Leftrightarrow [Fe_{1-x}, M_x]S(s) + xFe(II) \quad (1)$$

- Precipitation of MS following FeS dissolution

$$FeS(s) + M(II) \Leftrightarrow MS(s) + Fe(II) \quad (2)$$

To explain Cd(II) sorption by FeS, Coles et al. (2000) proposed the formation of $[Fe_{1-x}, Cd_x]S$ through lattice exchange, without the solid-phase characterization. For the formation of this solid solution, Cd(II) should fit into the Fe(II) sites of FeS. In mackinawite, each Fe^{2+} is surrounded by four sulfurs at 2.26 Å (Taylor and Finger 1970). CdS occurs as greenockite (hexagonal) or hawleyite (cubic) (Bostick et al. 2000). Although Cd^{2+} is coordinated by four sulfurs in these polymorphs, the Cd–S bonding distance (2.53 Å for greenockite and 2.52 Å for hawleyite) is considerably longer than the Fe–S distance in mackinawite (Makovicky 2006; Vaughan and Craig 1978), making the substitution of Cd^{2+} for Fe^{2+} on the FeS surface unlikely. Also, the significantly different solubilities of CdS and FeS would favor the formation of CdS through reaction (2) (Wilkin and Beak 2017). In contrast to our case, Wilkin and Beak (2017) found that Ni^{2+} substituted Fe^{2+} in FeS to form solid solutions ($[Fe_{1-x}, Ni_x]S$) because of the similar ionic radii and comparable solubilities of the metal sulfides. As discussed later, CdS formation was confirmed by XRD and TEM analyses. Also, Cd^{2+} does not co-precipitate with FeS (Framson and Leckie 1978). Without any substantial rearrangement on the FeS surface, CdS precipitation through reaction (2) better explains the increasing $[Fe(II)]_{diss}$ with $[Cd(II)]_0$ at pH < ~7.

At pH 5.5–6.0, Fig. 2a compares the amount of the liberated Fe(II) ($[Fe(II)]_{lib}$) to that of the sorbed Cd(II) ($[Cd(II)]_{sorb}$). Here, $[Fe(II)]_{lib}$ is given by the difference between $[Fe(II)]_{diss}$ and the FeS solubility. Thus, $[Fe(II)]_{lib}$ does not consider the resorption of Fe(II), which will be discussed in "Quantification of adsorption and precipitation" section. Our previous results of Hg(II) sorption are also included. In Fig. 2a, $[Fe(II)]_{lib}$ increased with the sorbed M(II) concentration ($[M(II)]_{sorb}$), supporting the occurrence of metal sulfide (MS) precipitation via reaction (2). If MS precipitation is solely responsible for the removal of Cd(II) and Hg(II) and the liberated Fe(II) is not subject to resorption, $[Fe(II)]_{lib}$ is the same as $[M(II)]_{sorb}$. In this case, the data should lie on the dashed line in Fig. 2a. However, $[Fe(II)]_{lib}$ was lower than $[M(II)]_{sorb}$. Similar results have been reported for Hg(II) sorption by metal sulfides (Jeong et al. 2007; Phillips and Kraus (1965). In addition to MS precipitation, adsorption was proposed to account for the removal of Cd(II) and Hg(II):

- Surface complexation with sulfhydryl functional sites (≡FeSH) on FeS:

$$\equiv FeSH + M(II) - L \Leftrightarrow \equiv FeS - M(II) - L + H^+ \quad (3)$$

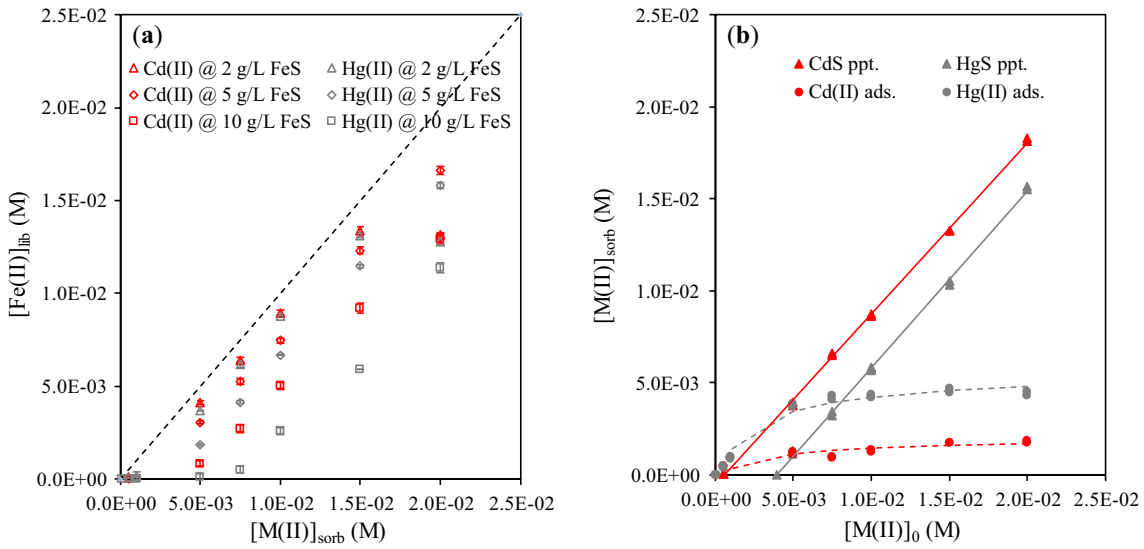

Fig. 2 Liberated Fe(II) concentration ($[Fe(II)]_{lib}$) versus sorbed M(II) concentration ($[M(II)]_{sorb}$) at pH 5.5–6.0 (**a**) and sorbed M(II) concentration ($[M(II)]_{sorb}$) versus initial M(II) concentration ($[M(II)]_0$) in 10 g/L FeS batches at pH 5.5–6.0 (**b**). In part **a**, error bars indicate one standard error. In part **b**, solid and dashed lines represent linear and Langmuir-like fits, respectively. Hg(II) sorption data are from Jeong et al. (2007)

- Surface complexation with hydroxyl functional sites (≡FeOH) on FeS:

$$\equiv \mathrm{FeOH} + \mathrm{M(II)} - \mathrm{L} \Leftrightarrow \equiv \mathrm{FeO} - \mathrm{M(II)} - \mathrm{L} + \mathrm{H}^{+} \quad (4)$$

where L represents ligands other than H_2O (e.g., OH^- and Cl^-). As indicated by reactions (3) and (4), adsorption does not lead to the liberation of Fe(II). Of these two, reaction (3) is preferred because of the greater affinity of both soft metal ions for sulfides than hydroxides (Stumm and Morgan 1995). In Fig. 2a, the vertical displacements between the data points and the dashed line indicate the contribution of adsorption; the larger the displacement, the greater the contribution of adsorption. In Fig. 2a, adsorption is more important at higher $[FeS]_0$ and lower $[M(II)]_0$ (note that $[M(II)]_0 \approx [Me(II)]_{sorb}$ given the nearly complete removal of M(II)). The observed importance of adsorption at lower surface loadings was consistent with the greater availability of surface functional sites per M(II) sorption.

In Fig. 2a, the $[Fe(II)]_{lib}$ resulting from Cd(II) sorption was higher than that from Hg(II) sorption, implying that MS precipitation was more important for the former. At first glance, this is not consistent with the higher solubility of CdS ($K_{sp} = 10^{-27.0}$) than HgS ($K_{sp} = 10^{-52.7}$) (Stumm and Morgan 1995). Chloride was found to hinder Hg(II) adsorption by forming aqueous Hg(II)-chloride complexes, which have lower affinities for sulfhydryl functional sites (≡FeSH) than Hg(II)-hydroxide complexes (Jeong et al. 2007; Sun et al. 2017). Therefore, the aqueous speciation of Cd(II) and Hg(II) was considered to explain their different sorption behaviors. However, under our experimental conditions, the thermodynamic calculations (Additional file 1: Fig. S4) show that chloride complexes were the dominant species for both metals. Thus, the aqueous phase speciation did not cause the aforementioned differences.

Instead, the thermodynamic stability of adsorbed Me(II) species (≡FeS–M(II)–L) formed by reaction (3) may control the relative contributions of adsorption and MS precipitation. For Hg(II) sorption by FeS, both TEM-EDS and Hg L_3-edge XAS analyses revealed the formation of Hg(II)-chlorosulfide surface complexes (Jeong et al. 2020). Similarly, our TEM-EDS analyses in "TEM" section indicate the presence of ≡FeS–Cd(II)–Cl. The stability of ≡FeS–M(II)–Cl can be inferred from that of the corresponding aqueous chlorosulfide complex. Unfortunately, no such information is available. Thus, the stability of ≡FeS–M(II)–Cl was determined using the formation constants of the following reactions (refer to Appendix 6.1 in Stumm and Morgan 1995):

$$\mathrm{Cd}^{2+} + \mathrm{S}^{2-} \Leftrightarrow \mathrm{CdS}^{o}, K\left(\mathrm{CdS}^{o}\right) = 10^{19.5} \quad (5)$$

$$\mathrm{Cd}^{2+} + \mathrm{Cl}^{-} \Leftrightarrow \mathrm{CdCl}^{+}, K\left(\mathrm{CdCl}^{+}\right) = 10^{2.0} \quad (6)$$

$$\mathrm{Hg}^{2+} + \mathrm{S}^{2-} \Leftrightarrow \mathrm{HgS}^{o}, K\left(\mathrm{HgS}^{o}\right) = 10^{7.9} \quad (7)$$

$$Hg^{2+} + Cl^- \Leftrightarrow HgCl^+, K\left(HgCl^+\right) = 10^{7.2} \quad (8)$$

Using the formation constants, the ratios of $K(CdS^o)/K(CdCl^+)$ and $K(HgS^o)/K(HgCl^+)$ were calculated to be $10^{17.5}$ and $10^{0.7}$, respectively. As the ratio is substantially greater than unity, M(II)-S bond becomes stronger than M(II)-Cl bond (i.e., the bonding distance of M(II)-S becomes shorter relative to that of M(II)-Cl), thus reducing the stability of ≡FeS–M(II)–Cl. When the ratio is close to unity, ≡FeS–M(II)–Cl is stable. Therefore, ≡FeS–Cd(II)–Cl is expected to be less stable than ≡FeS–Hg(II)–Cl, making adsorption less important for Cd(II) sorption. At pH > ~7, $[Fe(II)]_{diss}$ abruptly decreased due to significant resorption of the liberated Fe(II) (Fig. 1b). Under these pH conditions, thus, it was not possible to assess the relative importance of adsorption and MS precipitation.

Quantification of adsorption and precipitation

As aforementioned, it is possible to qualitatively assess the relative importance of adsorption and MS precipitation. In this section, the contributions of these mechanisms are determined in a quantitative way. At pH < ~7, the liberated Fe(II) can be resorbed through adsorption. According to Jeong et al. (2007), the Fe(II) sorption in 10 g/L FeS batches at pH 5.5–6.0 followed a Langmuir-like isotherm (Additional file 1: Fig. S5):

$$q_{Fe(II)} = \frac{q_{Fe(II),max} K_{ad} [Fe(II)]_{diss}}{1 + K_{ad} [Fe(II)]_{diss}} \quad (9)$$

where $q_{Fe(II)}$ is the adsorbed Fe(II) concentration; $q_{Fe(II),max}$ is the adsorption capacity of Fe(II); and K_{ad} is the adsorption coefficient. At pH 5.5–6.0, $q_{Fe,max}$ and K_{ad} were estimated to be 0.42 mmol/g and 3400 L/mol, respectively. Thus, the adsorption of the liberated Fe(II) should be considered to accurately determine the contributions of adsorption and MS precipitation. Otherwise, the former mechanism would be overestimated, while the latter would be underestimated. Assuming that the competitive adsorption between M(II) and Fe(II) is not substantial, the contribution of M(II) adsorption can be determined based on the molar balance of M(II):

$$q_{M(II)} = \frac{[M(II)]_{sorb} - [Fe(II)]_{lib}}{[FeS]_0} - q_{Fe(II)} \quad (10)$$

where $q_{M(II)}$ is the concentration of the adsorbed M(II). In this study, $[M(II)]_{sorb}$ was substituted with $[M(II)]_0$ because the initially added M(II) was almost completely immobilized. The numerator of the first term on the right-hand side of Eq. (10) corresponds to the vertical displacement in Fig. 2a. Once $q_{M(II)}$ is determined using Eq. (10), the contribution of MS precipitation is obtained by the difference between $[M(II)]_{sorb}$ and $q_{M(II)}$.

In Fig. 2b, the contribution of adsorption was compared to that of MS precipitation in 10 g/L FeS batches at pH 5.5–6.0. For both metals, the adsorption exhibited a Langmuir-like behavior, whereas MS precipitation followed a linear pattern. Consequently, the former became less important with $[M(II)]_0$. Moreover, the continued increase in MS precipitation in Fig. 2b indicates that the sorption capacity of FeS was not exhausted under our experimental conditions. As discussed in "Cd(II) sorption" section, adsorption contributed less to Cd(II) sorption than Hg(II) sorption. At pH 5.5–6.0, Cd(II) adsorption was more important than CdS precipitation when $[Cd(II)]_0/[FeS]_0 \leq 0.05$ mmol/g. In contrast, Hg(II) adsorption prevailed at $[Hg(II)]_0/[FeS]_0$ as high as 0.75 mmol/g. By using Langmuir isotherms, the adsorption capacities ($q_{M(II),max}$) of Cd(II) and Hg(II) at pH 5.5–6.0 were estimated to be 0.20 and 0.55 mmol/g, respectively. Also, the total adsorption capacities of Cd(II) and Hg(II), the sum of $q_{Fe(II),max}$ and $q_{M(II),max}$, accounted for 43 and 67% of the total sulfhydryl functional sites, respectively ($[\equiv SH]_T = 1.45$ mmol/g from Jeong (2005)). Given that a considerable fraction of the sulfhydryl sites remained unoccupied, the competitive adsorption between M(II) and the liberated Fe(II) was not significant. The resorption of the liberated Fe(II) would be overestimated because it was independently measured from Fe(II)-added FeS batches. Also, due to its lower affinity for sulfides than Cd(II) and Hg(II) (Stumm and Morgan 1995), Fe(II) tends to adsorb less selectively to sulfhydryl functional sites. Thus, M(II) adsorption is substantially underestimated if the competitive adsorption is significant.

XRD

XRD analyses were performed to examine crystalline products as a function of $[Cd(II)]_0/[FeS]_0$ and pH. In Fig. 3, the diffractograms of Cd(II)-added FeS batches are presented with those of halite (NaCl), mackinawite (FeS), greigite (Fe_3S_4), magnetite (Fe_3O_4), greenockite (CdS, hexagonal), and hawleyite (CdS, cubic). The intensity of the (001) reflection peak of mackinawite at $2\theta = 17.6°$ was dependent on $[Cd(II)]_0/[FeS]_0$ and pH. Its intensity became weaker at higher $[Cd(II)]_0/[FeS]_0$ due to the increased MS formation at the expense of FeS via reaction (2). For example, this peak almost disappeared at $[Cd(II)]_0/[FeS]_0 = 7.5$ mmol/g (Fig. 3a). At $[Cd(II)]_0/[FeS]_0 = 2.0$ and 0.1 mmol/g (Fig. 3b), the peak was weak at acidic pH, where FeS became increasingly soluble (Rickard 2006).

At $[Cd(II)]_0/[FeS]_0 = 7.5$ mmol/g, the peaks at $2\theta = 26.5°$, 43.9°, and 52.0° correspond to the (111),

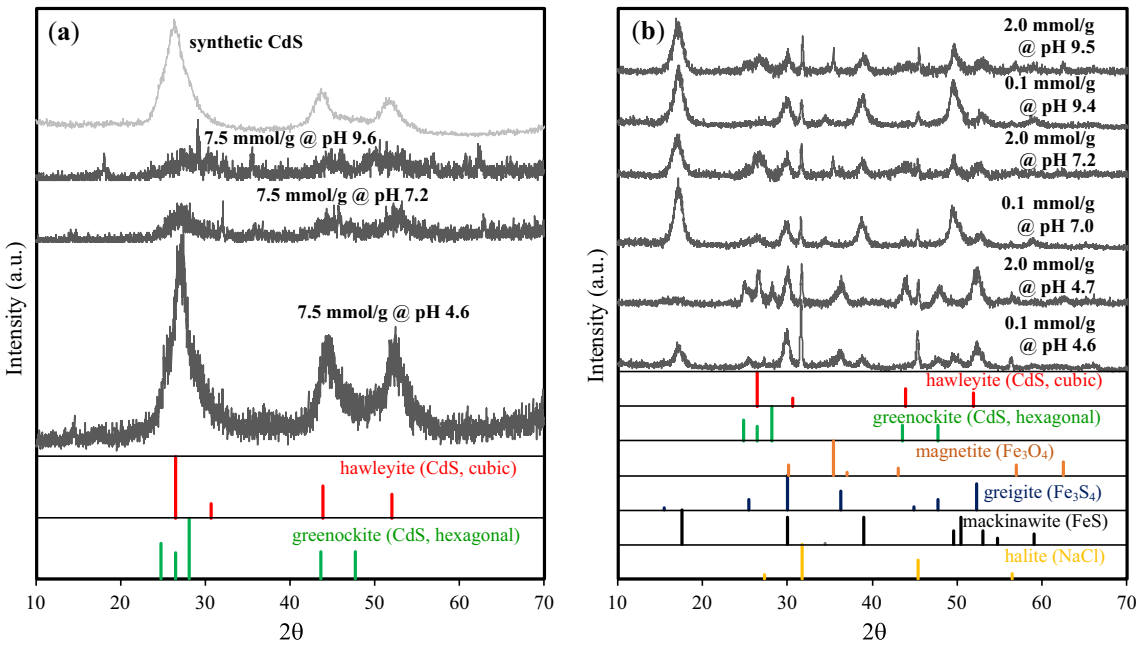

Fig. 3 X-ray diffraction (XRD) patterns of Cd(II)-added FeS batches at a high surface loading (**a**) and low surface loadings (**b**). The surface loadings ($[Cd(II)]_0/[FeS]_0$) and pH are indicated in the figure

(220), and (311) planes of hawleyite, respectively (Fig. 3a). These peaks were wide and diffused, indicating the nanocrystalline nature of hawleyite. In Fig. 3b, although the strongest (111) peak of hawleyite was present at $[Cd(II)]_0/[FeS]_0 = 2.0$ mmol/g, it was not evident at $[Cd(II)]_0/[FeS]_0 = 0.1$ mmol/g. This was likely due to less production of hawleyite. Previously, Bostick et al. (2000) observed the formation of hawleyite in Cd(II) sorption by amorphous FeS_2. In Fig. 3a, hawleyite was obtained by mixing Cd(II) and S(-II) solutions. The free energies of formation for hawleyite and greenockite are similar (Daskalakis and Helz 1992). At $[Cd(II)]_0/[FeS]_0 = 2.0$ mmol/g and pH = 4.7, the peaks at $2\theta = 24.8°$ and 28.1° matched the (100) and (101) planes of greenockite, respectively (Fig. 3b). In the other batches, although not identified by XRD, the formation of highly disordered greenockite could not be ruled out.

Greigite and magnetite were detected as Fe-bearing phases by XRD. In Fig. 3b, the first and second strongest reflection peaks of greigite at $2\theta = 30.0°$ and 52.4° coincide with the peaks of mackinawite; however, the third strongest peak at $2\theta = 36.4°$ does not overlap with the peaks of the other phases. With this peak, the presence of greigite was confirmed at acidic pH (Fig. 3b). For magnetite, the strongest peak at $2\theta = 35.5°$ was observed at neutral to basic pH at $[Cd(II)]_0/[FeS]_0 = 2.0$ mmol/g. Given the lack of strong oxidants in our batch systems, the formation of both Fe(II)–Fe(III) phases was unexpected. Instead, these Fe phases resulted from sample alterations during XRD measurements or freeze-drying. For the samples wetted by glycerin (Additional file 1: Fig. S6), the characteristic greigite peak at $2\theta = 36.4°$ was absent, indicating that this phase was produced during XRD measurements. However, even for the glycerin-treated samples at neutral to basic pH, the presence of magnetite was noted by the peak at $2\theta = 35.5°$ (Additional file 1: Fig. S6). Consequently, magnetite may be a direct resorption product of the liberated Fe(II) at pH > ~7. However, the followings negate this possibility. When probed using a magnet, the suspended particles in Cd(II)-added FeS batches were not ferromagnetic. In our previous study on Hg(II) sorption by FeS, magnetite was not detected in non-freeze-dried and glycerin-wetted samples by XRD (Jeong et al. 2007). Furthermore, the thermodynamic calculations (Additional file 1: Fig. S7) suggest that bulk Fe-bearing phases are unlikely to precipitate. Instead, chloride green rust-like surface precipitates would better explain the resorption of the liberated Fe(II). During freeze-drying, these surface precipitates were thought to become dehydrated and transform into magnetite.

TEM

TEM analyses can provide information on lattice fringe features, electron diffraction patterns, and the spatial distributions of elements. In Fig. 4, TEM images are shown with a SAED pattern. As the image contrast is

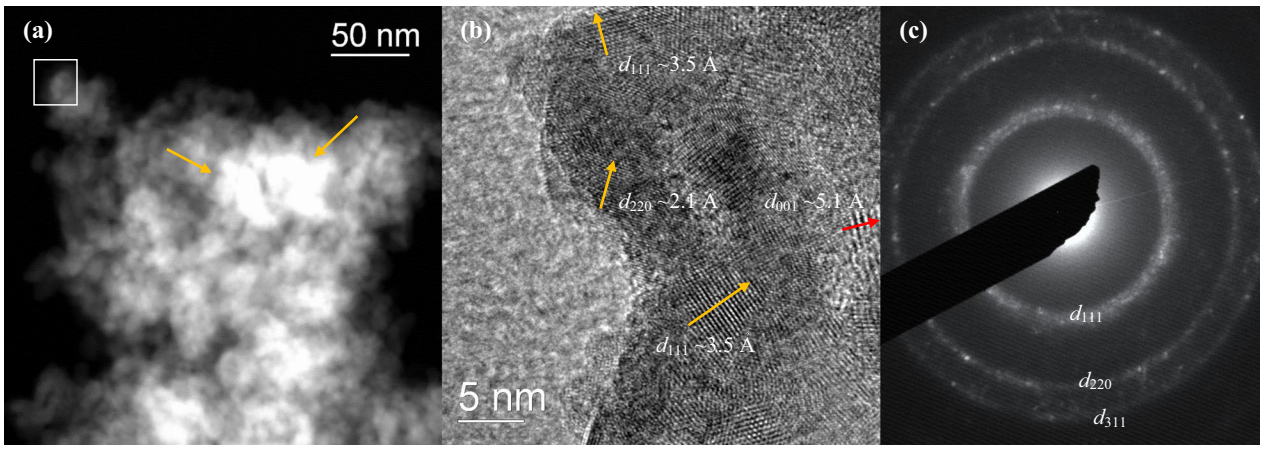

Fig. 4 High-angle annular dark-field scanning transmission electron microscopy (HAADF-TEM) image (**a**), high resolution-transmission electron microscopy (HR-TEM) image (**b**), and selected area electron diffraction (SAED) pattern (**c**). The sample was obtained from 0.015 M Cd(II)-added 2 g/L FeS batch at pH 4.6. Part **b** is an enlarged image of the boxed area in part **a**. In part **b**, orange arrows indicate the lattice fringe patterns of hawleyite, and the yellow arrow indicates those of mackinawite. In part **c**, the reflection rings are indexed for hawleyite

proportional to the square of the atomic number (Utsunomiya and Ewing 2003), the regions rich in the heaviest element, Cd, should be brighter in a dark-field image (Fig. 4a). Thus, the areas indicated by arrows are concentrated with Cd, which likely corresponds to CdS precipitates. The high-resolution image in Fig. 4b reveals the lattice fringe features of hawleyite and mackinawite. In this figure, the intensity modulations with the spacing of ~3.5 and ~2.1 Å are indicative of the (111) and (220) planes of hawleyite, respectively. The intensity modulations with a longer spacing (e.g., ~5.1 Å) result from the (001) plane of mackinawite. Notably, the FeS particle with these long-spaced modulations seems to be worn away due to the dissolution via reaction (2). Also, this particle is not structurally related to hawleyite particles. Taken together, hawleyite was formed by bulk precipitation following FeS dissolution, not by lattice exchange on the FeS surface. Despite intensive searches, fringe features were not observed for greenockite. The high surface loading in Fig. 4 may have favored the formation of hawleyite over greenockite (Bostick et al. 2000). The SAED pattern in Fig. 4c exhibits several diffraction rings, all of which correspond to hawleyite. Consistent with the XRD results, these rings were diffused, indicating the highly disordered nature of hawleyite.

Elemental maps of Cd, Fe, S, Cl, and O were collected using EDS (Additional file 1: Figs. S8–S10). Using these maps, spatial correlation analyses were conducted between the elements using ImageJ 1.42 (National Institutes of Health, USA) (Additional file 1: Figs. S11–S13), with the results summarized in Table 1. Relatively weak correlations were observed for the Cd-Fe pairs because both metal ions behaved as Lewis acids. Thus, the correlation coefficients (R) of these pairs can be used to judge how meaningfully the other pairs are spatially correlated.

Table 1 Spatial correlation analyses of dispersive X-ray spectroscopy (EDS) maps

Batch compositions	Linear correlations	
0.015 M Cd(II)-added 2 g/L FeS at pH 4.6	(a) $I_{Fe} = 0.01 + 0.37\ I_{Cd}$	$R = 0.77$
	(b) $I_S = 0.02 + 1.61\ I_{Fe}$	$R = 0.86$
	(c) $I_O = 0.00 + 0.21\ I_{Fe}$	$R = 0.79$
	(d) $I_S = 0.01 + 0.88\ I_{Cd}$	$R = 0.96$
	(e) $I_{Cl} = 0.00 + 0.14\ I_{Cd}$	$R = 0.91$
	(f) $I_O = 0.00 + 0.11\ I_{Cd}$	$R = 0.85$
0.015 M Cd(II)-addeded 2 g/L FeS at pH 7.2	(a) $I_{Fe} = 0.04 + 0.72\ I_{Cd}$	$R = 0.55$
	(b) $I_S = 0.05 + 0.38\ I_{Fe}$	$R = 0.53$
	(c) $I_O = 0.01 + 0.33\ I_{Fe}$	$R = 0.97$
	(d) $I_S = 0.00 + 0.91\ I_{Cd}$	$R = 0.98$
	(e) $I_{Cl} = 0.00 + 0.17\ I_{Cd}$	$R = 0.97$
	(f) $I_O = 0.02 + 0.26\ I_{Cd}$	$R = 0.58$
0.015 M Cd(II)-addeded 2 g/L FeS at pH 9.8	(a) $I_{Fe} = 0.13 + 0.62\ I_{Cd}$	$R = 0.43$
	(b) $I_S = 0.05 + 0.26\ I_{Fe}$	$R = 0.36$
	(c) $I_O = 0.00 + 0.29\ I_{Fe}$	$R = 0.96$
	(d) $I_S = 0.01 + 1.02\ I_{Cd}$	$R = 0.97$
	(e) $I_{Cl} = 0.00 + 0.13\ I_{Cd}$	$R = 0.94$
	(f) $I_O = 0.04 + 0.14\ I_{Cd}$	$R = 0.32$

I_X is the emission intensity of an element, X

For the Fe-S pairs, a strong correlation occurred at acidic pH, but poor correlations were observed at neutral to basic pH. The opposite trend was noted for the Fe–O pairs. At acidic pH, while small fractions of the liberated Fe(II) were resorbed by adsorption, the solid-phase

Fe was mostly present in the FeS remnants. However, at neutral to basic pH, nearly all the liberated Fe(II) was re-immobilized by forming Fe (oxyhydr)oxide-like phases, thus leading to strong associations of Fe with O.

The spatial correlations of Cd with anionic species (e.g., S, Cl, and O) can provide clues to its coordination environment. First, strong correlations of the Cd-S pairs represent either CdS precipitation or Cd(II) adsorption to sulfhydryl functional sites. Second, strong correlations were observed for the Cd-Cl pairs. Because the dissolved Cd(II) was undersaturated with respect to $CdCl_2$ and Cd(OH)Cl, the Cd-Cl correlations correspond to the adsorption of chloride-complexed Cd(II). Given the strong correlations of both the Cd-S and Cd-Cl pairs, the adsorbed Cd(II) would occur as chlorosulfide-like forms (≡FeS–Cd(II)–Cl). Third, a significant correlation of the Cd–O pair was observed only at acidic pH. In 0.015 M Cd(II)-added 2 g/L FeS batches, the sorption capacity of Cd(II) approached the saturation limit at acidic pH (Fig. 1a). Thus, at acidic pH, the sulfhydryl functional sites became completely occupied, rendering hydroxyl functional sites available for Cd(II) adsorption.

Conclusions

This study demonstrated that mackinawite is effective for sequestering Cd(II) under anoxic conditions. By reaction with FeS, Cd(II) was immobilized through adsorption and CdS precipitation, with their relative importance dependent on $[Cd(II)]_0/[FeS]_0$. The former was dominant at low $[Cd(II)]_0/[FeS]_0$, and the latter became important at high $[Cd(II)]_0/[FeS]_0$. The surface loadings examined can encompass various contamination scenarios. Low surface loadings can be related to Cd contamination in sulfide-rich environments, such as estuarine sediments and marine environments. Consistent with the dominance of adsorption at low surface loadings, the dissolved Cd in anoxic marine basins (e.g., the Black Sea and Framvaren Fjord) was undersaturated with respect to CdS (Daskalakis and Helz, 1992). High surface loadings can simulate contamination scenarios at mine tailings and industrial waste disposal sites. In groundwater, continuous flows with even low levels of Cd(II) contamination eventually saturate the sorption capacity of FeS, thus resulting in the conditions that are better described by high surface loadings. To this end, this study provides mechanistic insights into Cd(II) sorption under various contamination scenarios.

The elucidation of sorption mechanisms is of environmental importance as they determine the stability of sorbed Cd(II) and its susceptibility to remobilization under dynamic geochemical conditions. Compared to Hg(II) sorption, Cd(II) sorption by FeS was more contributed to by MS precipitation than adsorption. Under oxidizing conditions, while the Cd(II) species adsorbed onto FeS are readily remobilized, CdS is more resistant to oxidation than FeS (Simpson et al. 1998). Given the prevalence of CdS precipitation, FeS can provide a better sink for Cd(II) even under oxidizing conditions.

Supplementary Information

The online version contains supplementary material available at https://doi.org/10.1186/s40543-022-00359-w.

Additional file 1: Figure S1 X-ray diffraction (XRD) patterns of as-synthesized FeS with Cu-Kα radiation. Diffraction peaks are indexed according to diffraction pattern of mackinawite. **Figure S2** Time profiles of dissolved Fe(II) and Cd(II) concentrations at pH 4.9 (a) and 9.1 (b) in 0.01 M Cd(II)-added 10 g/L FeS batches. **Figure S3** Sorbed Cd(II) concentration ($[Cd(II)]_{sorb}$) versus initial Cd(II) concentration ($[Cd(II)]_0$) at pH 5.5–6.0 (a) and 9.5–10.0 (b). **Figure S4** Aqueous speciation of Cd(II) (a) and Hg(b) determined by MINEQL + 4.5 (Environmental Research Software) under the condition of initial M(II) concentration ($[M(II)]_0$) at 0.015 M and total chloride concentration (Cl_T) at 0.2 M. In part (a), OH-complexes are $CdOH^+$, $Cd(OH)_2^o$, $Cd(OH)_3^-$, $Cd(OH)_4^{2-}$, and Cd_2OH^{3+}; and Cl-complexes are $CdCl^+$, $CdCl_2^o$, $CdCl_3^-$, and $CdOHCl^o$. In part (b), OH-complexes are $HgOH^+$, $Hg(OH)_2^o$, and $Hg(OH)_3^-$; and Cl-complexes are $HgCl^+$, $HgCl_2^o$, $HgCl_3^-$, $HgCl_4^{2-}$, and $HgOHCl^o$. **Figure S5** Fe(II) adsorption in 10 g/L FeS batches at pH 5.5–6.0. While $q_{Fe(II)}$ is adsorbed Fe(II) concentration, $[Fe(II)]_{diss}$ is dissolved Fe(II) concentration. Solid line represents the fit of a Langmuir isotherm. Sorption data are from Jeong et al. (2007). **Figure S6** X-ray diffraction (XRD) patterns of the samples that were freeze-dried and then wetted with glycerin. The samples were Cd(II)-reacted FeS batches with the surface loading of Cd(II) ($[Cd(II)]_0/[FeS]_0$) at 2.0 mmol/g. **Figure S7** Measured dissolved Fe concentrations versus estimated Fe concentrations from the solubility of $Fe(OH)_2$, chloride green rust, magnetite, and ferrihydrite along the measured (pH, Eh) couples. Measured data are from 0.01 M Cd(II)-added 10 g/L FeS at $Cl_T = 0.2$ M. Thermodynamic calculations were made by using MINEQL + 4.5. **Figure S8** Transmission electron microscopy image (a) and its dispersive X-ray spectroscopy (EDS) maps of Cd (b), Fe (c), S (d), Cl (e), and O (f). The sample was from 0.015 M Cd(II)-reacted 2 g/L FeS batch at pH 4.6. **Figure S9** Transmission electron microscopy image (a) and its dispersive X-ray spectroscopy (EDS) maps of Cd (b), Fe (c), S (d), Cl (e), and O (f). The sample was from 0.015 M Cd(II)-reacted 2 g/L FeS batch at pH 7.2. **Figure S10** Transmission electron microscopy image (a) and its dispersive X-ray spectroscopy (EDS) maps of Cd (b), Fe (c), S (d), Cl (e), and O (f). The sample was from 0.015 M Cd(II)-reacted 2 g/L FeS batch at pH 9.8. **Figure S11** Spatial correlations of Cd versus Fe (a), Fe versus S (b), Fe versus O (c), Cd versus S (d), Cd versus Cl (e), and Cd versus O (f). The EDS maps are from **Fig. S8** (0.015 M Cd(II)-reacted 2 g/L FeS batch at pH 4.6). **Figure S12** Spatial correlations of Cd versus Fe (a), Fe versus S (b), Fe versus O (c), Cd versus S (d), Cd versus Cl (e), and Cd versus O (f). The EDS maps are from **Fig. S9** (0.015 M Cd(II)-reacted 2 g/L FeS batch at pH 7.2). To emphasize the Fe associations with S, the red line in part (b) is identical to the regression line in **Fig. S11b**. **Figure S13** Spatial correlations of Cd versus Fe (a), Fe versus S (b), Fe versus O (c), Cd versus S (d), Cd versus Cl (e), and Cd versus O (f). The EDS maps are from **Fig. S10** (0.015 M Cd(II)-reacted 2 g/L FeS batch at pH 9.8). To emphasize the Fe associations with S, the red line in part (b) is identical to the regression line in **Fig. S11b**.

Acknowledgements
We appreciate Dr. Hayes for his technical support.

Author contributions
All authors contributed to the study conception and design. Material preparation, data collection and analysis were performed by MP, K-SL, JR, Y-SS and HYJ. While the first draft of the manuscript was written by MP, it was

thoroughly reviewed and revised by HYJ. All authors read and approved the final manuscript.

Funding
This work was supported by Basic Science Research Program through the Basic Research Project of Korea Institute of Geoscience and Mineral Resources (20-3412-1), National Research Council of Science & Technology grant by Korea government (MSIP) (CAP-17-05-KIGAM), and the Basic Science Research Program through the National Research Foundation of Korea (NRF-2021R1A2C1004455).

Availability of data and materials
All data generated or analyzed during this study are included in this published article and its supplementary information file.

Declarations

Competing interests
The authors declare that they have no competing interests.

Author details
[1]Department of Geological Sciences, BK21 School of Earth and Environmental Systems, Pusan National University, Busan 46241, South Korea. [2]Research Center for Geochronology & Isotope Analysis, Korea Basic Science Institute, Ochang, Chungbuk 28119, South Korea. [3]Geologic Environment Research Division, Korea Institute of Geoscience and Mineral Resources (KIGAM), Daejeon 34132, South Korea.

Received: 27 September 2022 Accepted: 28 November 2022
Published online: 16 December 2022

References

Benning LG, Wilkin RT, Barnes HL. Reaction pathways in the Fe–S system below 100 °C. Chem Geol. 2000;167:25–51.
Bostick BC, Fendorf S, Fendorf M. Disulfide disproportionation and CdS formation upon cadmium sorption on FeS_2. Geochim Cosmochim Acta. 2000;64:247–55.
Chen X, Wright JV, Conca JL, Peurrung LM. Effects of pH on heavy metal sorption on mineral apatite. Environ Sci Technol. 1997;31:624–31.
Chen D, Wang X, Wang X, Feng K, Su J, Dong J. The mechanism of cadmium sorption by sulphur-modified wheat straw biochar and its application cadmium-contaminated soil. Sci Total Environ. 2020;714:136550.
Coles CA, Rao SR, Yong RN. Lead and cadmium interactions with mackinawite: retention mechanisms and the role of pH. Environ Sci Technol. 2000;34:996–1000.
Daskalakis KD, Helz GR. Solubility of CdS (greenockite) in sulfidic waters at 25 °C. Environ Sci Technol. 1992;26:2462–6.
Di Toro DM, Mahony JD, Hansen DJ, Scott KJ, Hicks MB, Mayr SM, Redmond MS. Toxicity of cadmium in sediments: the role of acid volatile sulfide. Environ Toxicol Chem. 1990;9:1487–502.
Di Toro DM, Mahony JD, Hansen DJ, Berry WJ. A model of the oxidation of iron and cadmium sulfide in sediments. Environ Toxicol Chem. 1996;15:2168–86.
Dulnee S, Scheinost AC. Interfacial reaction of Sn^{II} on mackinawite (FeS). J Contam Hydrol. 2015;177–178:183–93.
Framson PE, Leckie JO. Limits of coprecipitation of cadmium and ferrous sulfides. Environ Sci Technol. 1978;12:465–9.
Genchi G, Sinicropi MS, Lauria G, Carocci A, Catalano A. The effects of cadmium toxicity. Int J Environ Res Public Health. 2020;17:3782.
Goldhaber MB, Kaplan IR. The sulfur cycle. In: Goldberg ED, editor. The sea. New York: Wiley-Interscience; 1974. p. 569–655.
Guilbaud R, Butler IB, Ellam RM, Ricjard D. Fe isotope exchange between $Fe(II)_{aq}$ and nanoparticulate mackinawite (FeS_m) during nanoparticle growth. Earth Planet Sci Lett. 2010;300:174–83.
Jean GE, Bancroft GM. Heavy metal adsorption by sulphide minerals. Geochim Cosmochim Acta. 1986;50:1455–63.
Jeong HY, Hayes KF. Impact of transition metals on reductive dechlorination rate of hexachloroethane by mackinawite. Environ Sci Technol. 2003;37:4650–5.
Jeong HY, Klaue B, Blum JD, Hayes KF. Sorption of mercuric ion by synthetic nanocrystalline mackinawite (FeS). Environ Sci Technol. 2007;41:7699–705.
Jeong HY, Lee JH, Hayes KF. Characterization of synthetic nanocrystalline mackinawite: crystal structure, particle size, and specific surface area. Geochim Cosmochim Acta. 2008;72:493–505.
Jeong HY, Sun K, Hayes KF. Microscopic and spectroscopic characterization of Hg(II) immobilization by mackinawite (FeS). Environ Sci Technol. 2020;44:7476–83.
Kubier A, Wilkin RT, Picher T. Cadmium in soils and groundwater: a review. Appl Geochem. 2019;108:104388.
Larison RJ, Likens GE, Fitzpatrick JW, Crook JG. Cadmium toxicity among wildlife in the Colorado rocky mountains. Nature. 2000;406:181–3.
Liang X, Xu Y, Sun G, Wang L, Sun Y, Qin X. Preparation, characterization of thiol-functionalized silica and application for sorption of Pb^{2+} and Cd^{2+}. Colloids Surf A Physicochem Eng Asp. 2009;349:61–8.
Lusvardi G, Malavasi G, Menabue L, Saladini M. Removal of cadmium ion by means of synthetic hydroxyapatite. Waste Manage. 2002;22:853–7.
Makovicky E. Crystal structures of sulfides and other chalcogenides. Rev Mineral Geochem. 2006;61:7–125.
Malferrari D, Brigatti MF, Laurora A, Pini S, Medici L. Sorption kinetics and chemical forms of Cd(II) sorbed by thiol-functionalized 2:1 clay minerals. J Hazard Mater. 2007;143:73–81.
Moore JW, Ramamoorthy S. Cadmium. In: Moore JW, editor. Heavy metals in natural waters-applied monitoring and impact assessment. Berlin: Springer; 1984. p. 28–57.
Morse JW, Arakaki T. Adsorption and coprecipitation of divalent metals with mackinawite (FeS). Geochim Cosmochim Acta. 1993;57:3635–40.
Ohfuji H, Rickard D. High resolution transmission electron microscopic study of synthetic nanocrystalline mackinawite. Earth Planet Sci Lett. 2006;241:227–33.
Özverdi A, Erdem M. Cu^{2+}, Cd^{2+} and Pb^{2+} adsorption from aqueous solutions by pyrite and synthetic iron sulphide. J Hazard Mater. 2006;137:626–32.
Panuccio MR, Sorgonà A, Rizzo M, Cacco G. Cadmium adsorption on vermiculite, zeolite and pumice: batch experimental studies. J Environ Manage. 2009;90:364–74.
Papelis C. X-ray photoelectron spectroscopic studies of cadmium and selenite adsorption on aluminum oxides. Environ Sci Technol. 1995;29:1526–33.
Parkman RH, Charnock JM, Bryan ND, Livens FR, Vaughan DJ. Reactions of copper and cadmium ions in aqueous solution with goethite, lepidocrocite, mackinawite, and pyrite. Am Mineral. 1999;84:407–19.
Phillips HO, Kraus KA. Adsorption on inorganic materials: VI. Reaction of insoluble sulfides with metal ions in aqueous media. J Chromatogr A. 1965;17:549–57.
Pirveysian M, Ghiaci M. Synthesis and characterization of sulfur functionalized graphene oxide nanosheets as efficient sorbent for removal of Pb^{2+}, Cd^{2+}, Ni^{2+} and Zn^{2+} ions from aqueous solution: a combined thermodynamic and kinetic studies. Appl Surf Sci. 2018;428:98–109.
Rickard DT. Kinetics and mechanism of the sulfidation of goethite. Am J Sci. 1974;274:941–52.
Rickard D. The solubility of FeS. Geochim Cosmochim Acta. 2006;70:5779–89.
Simpson SL, Apte SC, Batley GE. Effect of short-term resuspension events on trace metal speciation in polluted anoxic sediments. Environ Sci Technol. 1998;32:620–5.
Song H, Kumar A, Zhang Y. A novel approach for the removal of Pb^{2+} and Cd^{2+} from wastewater by sulfur-ferromagnetic nanoparticles (SFMNs). Chemosphere. 2022;287: 132156.
Stumm W, Morgan JJ. Aquatic chemistry: chemical equilibria and rates in natural waters. 3rd ed. New York: Wiley; 1995.
Sun Y, Lv D, Zhou J, Zhou X, Lou Z, Baig SA, Xu X. Adsorption of mercury (II) from aqueous solutions using FeS and pyrite: a comparative study. Chemosphere. 2017;185:452–61.
Tan P, Hu Y, Bi Q. Competitive adsorption of Cu^{2+}, Cd^{2+} and Ni^{2+} from an aqueous solution on graphene oxide membranes. Colloids Surf A: Physicochem Eng Asp. 2016;509:56–64.
Taylor LA, Finger LW. Structural refinement and composition of mackinawite. Carnegie Inst Wash Geophys Lab Annu Rep. 1970;69:318–22.

Utsunomiya S, Ewing RC. Application of high-angle annular dark field scanning transmission electron microscopy, scanning transmission electron microscopy-energy dispersive X-ray spectrometry, and energy-filtered transmission electron microscopy to the characterization of nanoparticles in the environment. Environ Sci Technol. 2003;37:786–91.
Vaughan DJ, Craig JT. Mineral chemistry of metal sulfides. Cambridge: Cambridge University Press; 1978.
Wilkin RT, Beak DG. Uptake of nickel by synthetic mackinawite. Chem Geol. 2017;462:15–29.
Jeong HY. Removal of heavy metals and reductive dechlorination of chlorinated organic pollutants by nanosized FeS. Ph.D. Dissertation. Ann Arbor: University of Michigan; 2005.

Publisher's Note